Indian Journal of Pure & Applied Physics
Vol. 62, July 2024, pp. 614-619
DOI: 10.56042/ijpap.v62i7.7027

Different Morphological Features of Sulphidation Induced MoG Solid Spheres and Phase Mixing in Ball-in-Ball MoS_2 Heterostuctures

Angom Devadatta Mani
Department of Basic Science (Physics),
Manipur Technical University, Government Polytechnic Campus, Takyelpat, Imphal-West, Manipur 795 004, India

Received 30 November 2023; accepted 20 May 2024

Tailoring the morphological features of nanomaterials is of great importance for varied applications in energy storage, environment remediation etc. but is hampered by different parameters. Herein, a novel step by step synthesis approach is reported to elucidate different morphology of MoS_2 heterostructures. A solvothermal method is employed to synthesize molybdenum glycerate (MoG) solid spheres (SS) followed by subsequent sulphidation. Continuous sulphidation of 3 hours and 8 hours produces flowers and ball-in-ball MoS_2 heterostructures respectively. FESEM micrographs show the formation of MoG SS and different MoS_2 heterostructures. XRD, Raman and UV measurements confirm the phase transition from 2H (semiconductor) to 1T (metallic) phase in 8 hours sulphidated ball-in-ball heterostructure. The formation of ball-in-ball morphology is attributed to the Kirkendall effect. The findings could potentially be extended to the idea of phase transitions and their applications.

Keywords: Sulphidation; Phase transition; Kirkendall effect; Ball-in-ball heterostructures

1 Introduction

In recent years, atomically thin 2D materials, such as graphene, hexagonal boron nitride (h-BN), and the transition metal dichalcogenides (TMDs) have attracted much interest in both fundamental studies and applications. Among them, TMDs with the chemical formula MX_2 (X=S, Se, Te and M = transition metal) find a place as fascinating units for optoelectronic applications. TMDs are layered structures with strong in-plane covalent bonds however, a weak interlayer van der Waals (vdW) exists between the layers[1-3]. The exfoliation into a monolayer or thin layer becomes easier making them optically transparent and flexible. The fabrication of TMD-based devices is easier and durable compared to other devices. Further, the bandgap of most semiconducting TMDs is inversely proportional to the number of layers. A transition from indirect to a direct semiconductor is seenas the number of layers reduces to single layer, due to the interlayer decoupling and quantum confinement effects[4-6]. Out of all TMDs, MoS_2 layered nanostructures exist as three different polymorphs viz. 1T MoS_2, 2H MoS_2, and 3R MoS_2. Each polymorph shows ironical properties and has different applications. The metallic 1T phase and semiconducting 2H phase, show distinctive differences in their physical and chemical properties, especially the conductivity properties, where the metallic phase has ≈ 105 times electrical conductivity compared to the semiconducting phase[7-8]. The low electrical conductivity of semiconducting MoS_2 limits electrochemical energy storage applications[9]. However, due to its high stability and well developed synthesis approach, 2H MoS_2 is still the most popular MoS_2 phase in energy storage and conversion fields in most of the studies nowadays[10-11]. 2H MoS_2 is a very promising anode material for lithium or sodium-ion batteries, owing to its high theoretical specific capacity (670 mA h g-1) and low cost[12]. To facilitate easy electron transport in the 2H MoS_2, additional conductive additives such as graphene, carbon nanotubes, and carbon black are usually incorporated, which increase its cost, limit the rate performance, and decrease the active material loading. Compared to the 2H phase of MoS_2, the 1T phase has superior electron transfer capability due to its significantly higher electronic conductivity[12]. Consequently, using 1T MoS_2 as an electrode will minimize or even eliminate the addition of any further conductive additives and simultaneously achieve an excellent rate performance on energy storage fields[8]. Furthermore,

*Corresponding author:
(E-mail: angomdevadattamani@gmail.com)\

previous studies found that the basal plane of semiconducting 2H phase MoS_2 is catalytically inert for hydrogen evolution reaction (HER), whereas the basal planes of metallic 1T MoS_2 are rich in active sites. This will have the benefit of higher reaction kinetics between electrons and protons (H+) on the active sites and makes the 1T MoS_2 more promising candidate for energy generation and conversion fields[13-14]. Methods for re-engineering MoS_2 through new metallic structures that can solve the intrinsic problems of conductivity and catalytic activities have been developed[8]. Till now, different researchers have already reported many fabrication methods to obtain high purity metallic MoS_2. Usually, there are two kinds of fabrication methods: a top-down approach such as bulk MoS_2 exfoliation by alkali metal intercalation; and a bottom-up approach, such as hydrothermal and solvothermal synthesis[15]. In the Li intercalation method, the long lithiation duration and the use of expensive and highly reductive organometallic compounds require high vacuum processing environment which on leakage may be fatal. In addition, electron beam irradiation, pressure-induced, hot plasmonic electrons, sulphur-catalyzed, strain-induced, Na intercalation, Ar plasma induced, annealing on Au and Cu substrates, carbon doping, Pd addition, MXenes interfacing, H^+ regulated and Re assisted 2H to 1T MoS_2 phase transition were also reported so far[10,16-23]. Still, there is a great demand for a more versatile, low cost, scalable, clean novel strategies to enhance the applicability of phase transition in 2D materials.

In this work, a facile solvothermal method is employed to synthesize different MoS_2 heterostructures. Molybdenum glycerate (MoG) solid spheres (SS) were previously synthesized followed by sulphidation for 3h and 8h consecutively. Flower and ball-in-ball decorated MoS_2 heterostructures were observed for 3h and 8h sulphidated MoS_2 respectively. Mixing of semiconductor-2H and metallic-1T phases has been observed for ball-in-ball morphology. Metallic MoS_2 can be well distinguished from semiconducting MoS_2 by their prominent differences in the morphologies and structures. Different characterization techniques such as XRD, FESEM, Raman spectra, UV-VIS optical absorption were used to differentiate the distinct morphological features of metallic MoS_2 from that of semiconducting MoS_2. Herein, a dual purpose of morphology and phase transition is achieved simultaneously for 8h sulphidated ball-in-ball MoS_2. The highly conductive 1T MoS_2 would effectively enhance the performance of the MoS_2-based applications in energy storage and environmental remediation[24].

2 Experimental

Analytical grade chemicals were used directly without any further purification. A stoichiometric amount of MoO^2 $(acac)_2$ (Damas-beta, China) is dispersed in 10 ml of glycerol (Mreda, USA) followed by the addition of isopropyl-DI water mixture in the ratio of 3:1. The solution mixture is then transferred to a teflon lined autoclave at 200 °C for 8 h. The brownish solution is filtered out and the product so obtained is washed with ethanol 3 times to get Mo-glycerate (MoG) solid spheres (SS). Then, 20 g of MoG SS is dispersed in ethanol and allowed to undergo sulphidation by adding thioacetamide (TAA) (Macklin, China). The mixture is then transferred to the autoclave at 210 °C for several hours to get several morphology of MoS_2. The evolution of different hetero- structures with sulphidation time is shown in Fig. 1. MoS_2 flowers are decorated over the surface of MoG SS after sulphidation for 3h. A yolk-shell and consequently ball-in-ball heterostructures of MoS_2 are formed after 6h and 8h of sulphidation respectively The formation and phase identification of MoG and MoS_2 were characterized by the X-ray diffractometer (Bruker AXS, WI, USA) using Cu Kα radiation (λ = 1.5418 Å). Structural deformation and phase transition wereobserved from the Raman spectroscope (Invia Reflex, Reninshaw). The morphological features of the samples were characterized by the field emission scanning electron microscope (FESEM, SU-70, Hitachi, Japan). The absorption spectra of all

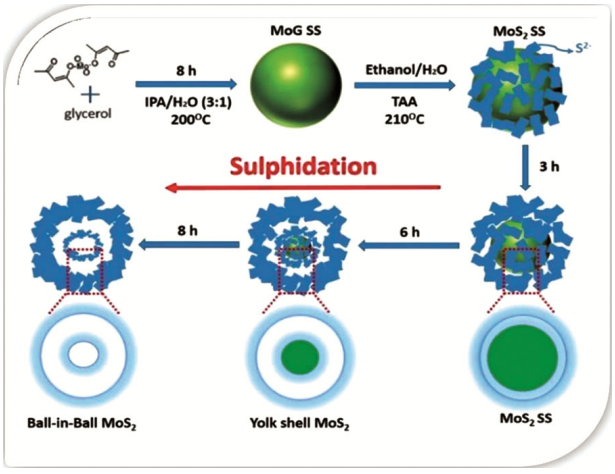

Fig. 1 — Schematic diagram showing different stages of MoS_2 synthesis

the samples were observed by an ultra-violet-visible spectrophotometer (Lambda 950, Perkin Elmer, USA).

3 Results and Discussion

3.1 XRD Analysis

Figure 2(a) shows the XRD pattern of MoG, 3h and 8h sulphidated MoS_2 heterostructures. Upon sulphidation, the intensity of MoG phases starts reducing however, the phases of MoS_2 are becoming more prominent. A broader peak and slight shift in peak position towards the lower 2θ region is observed near 32° for 8h sulphidated MoS_2 as compared to the 3h sulphidated sample. This suggests the possible phase mixing of 2H and 1T polymorphs for 8h sulphidated MoS_2. Fig. 2(b & c) compare the XRD pattern of freshly prepared MoG and 8h sulphidated MoS_2 with the reported patterns viz. JCPDS- 32-672 and JCPDS-37-1492. Hence, the formation of MoG and MoS_2 heterostructures is predicted from the XRD analyses[13].

3.2 Raman Analysis

Figure 3(d) shows the Raman spectra of 3h and 8h sulphidated MoS_2 heterostructures. The characteristic peaks of 3h sulphidated MoS_2 at 377 cm^{-1} (E^1, due to opposite vibration of two S atoms with respect to the Mo atom) and 404 cm^{-1} (A^1, associated with the

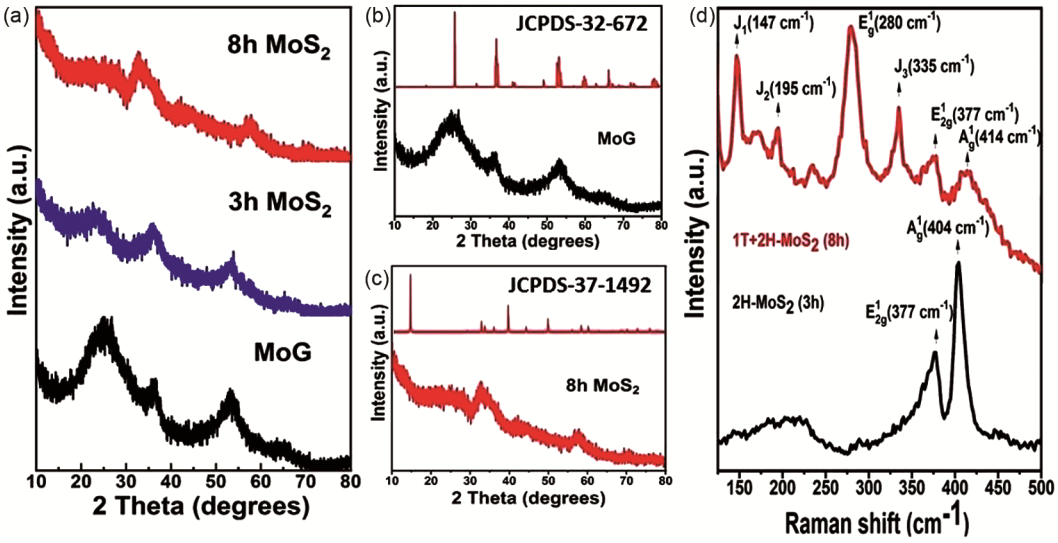

Fig. 2 — (a) XRD pattern of MoG, 3h and 8h sulphidated MoS_2, (b) Comparision of XRD pattern of MoG SS and JCPDS-32-572, (c) Comparision of XRD pattern of 8h sulphidated MoS_2 and JCPDS-37-1492, and (d) Raman spectra of 3h and 8h MoS_2

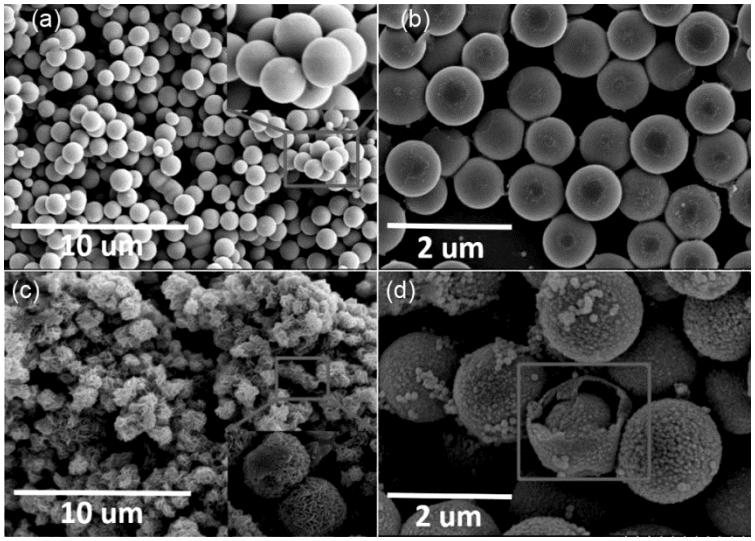

Fig. 3 — (a) FESEM micrograph and the resolved image of MoG SS, (b) MoS_2 after 30 min of sulphidation, (c) MoS_2 after 3h of sulphidation and resolved image is shown in the inset, and (d) MoS_2 after 8h of sulphidation

vibration of only S atoms in opposite direction) exhibit the semiconducting or 2H-MoS_2. The incorporation of metallic or 1T phases is observed for 8h sulphidated MoS_2. The signature of 1T structure in the Raman spectra appears at around 147, 195, 280 and 335 cm^{-1}, corresponding to J1, J2, E^1 and J3 respectively. Among them, E^1 band is related to the octahedral coordination of Mo in 1T MoS_2. The formation of 1T in 2H is usually judged by the appearance of J1, J2, E^1 and J3 modes. In this case, A^1 mode is present in both 2H and 1T structure, however, the peak is shifted from 404 cm^{-1} to 414 cm^{-1}. This confirms the phase transition from pure 2H to 1T-2H phase mixture. The phase purity of 1T structure is determined by the intensity of the characteristic E^1 peak of 2H MoS_2[13-14, 25].

3.3 SEM Analysis

Figure 3 (a) shows the FESEM image of MoG SS and the resolved image in the inset. The formation of grains in the form of solid spheres (SS) is observed throughout the sample which is a pivotal stage in the synthesis process. The use of glycerol sufficiently reduced the surface area of the grains to form solid spheres (SS)[26-28]. The average diameter of the spherical grains is ~ 700 nm. Fig. 3(b) shows the FESEM micrograph of 30 min sulphidated MoG SS. The conversion of MoG SS into MoS_2 heterostructures over the surface is not significant due to the short duration of sulphidation. Fig. 3(c) shows the formation of MoS_2 nanoflowers after 3h of sulphidation. The resolved image is shown in the inset. Further, an increase in sulphidation time ~ 6h may result in the formation of yolk-shell MoS_2 heterostructures. Finally, the formation of ball-in-ball MoS_2 heterostructures is shown in Fig. 3(d) after 8h of sulphidation. The change in different heterostructures with sulphidation time is diagrammatically shown in Fig. 1. The formation of ball-in-ball morphology is attributed to the Kirkendall effect[29]. According to it, the unequal diffusion rates between two interdiffusion atomic species create a vacancy or void near the interface during the fabrication process. In this case, metal (M) ions diffuse outwards and oxygen (O) ions diffuse inwards. During the process, a continuous layer of metal-oxygen (M-O) bonds is formed near the interface. Due to the slower diffusion of O compared to M, this layer is oxygen-deficient. This unbalanced diffusion creates oxygen vacancies leading to the formation of Kirkendall holes (KH) near the interface in the higher diffusion side[30]. During the early stage up to 6 hours of sulphidation, these holes are not sufficient enough to generate a complete hollow nanostructure, instead forming a yolk-shell heterostructure. Under continuous sulphidation for 8 hours, the outward flux of metal (M) ions from the core is sufficiently larger than the inward flux of oxygen (O) ions from the shell to form a hollow nanostructure. Hence, a ball-in-ball MoS_2 heterostructure is formed giving rise to a large surface area suitable for various related applications such as energy storage and catalytic systems[31-32].

3.3 UV Measurements

Figure 4(a) shows the UV-vis absorption spectra of 3h and 8h sulphidated MoS_2. The absorption spectra of 3h sulphidated MoS_2 possess some notable peaks in the visible spectrum illustrating its semiconducting behavior of 2H MoS_2. However, for 8h sulphidated MoS_2, the intensity of peaks in these regions decreases suggesting the decrease in the 2H phase and probable combination of the metallic 1T phase along with the semiconducting 2H phase. The metallic or semiconducting behavior of a material can also be predicted by the values of energy band gap (E_g) as obtained from the Tauc relation given by

$$\alpha h\nu = B(h\nu - Eg) \quad \ldots (1)$$

where α, B, hν are the absorption coefficient, constant and energy of the photon respectively and n

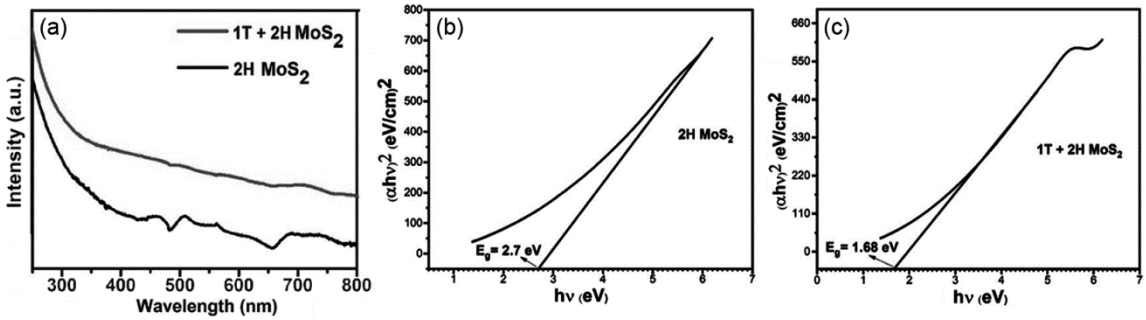

Fig. 4 — (a) Optical absorption spectra of 3h (2H) and 8h (1T + 2H) sulphidated MoS_2, (b) Tauc plot to find out the energy band gap of 3h (2H) and (c) Tauc plot to find out the energy band gap of 8h (1T + 2H) sulphidated MoS_2

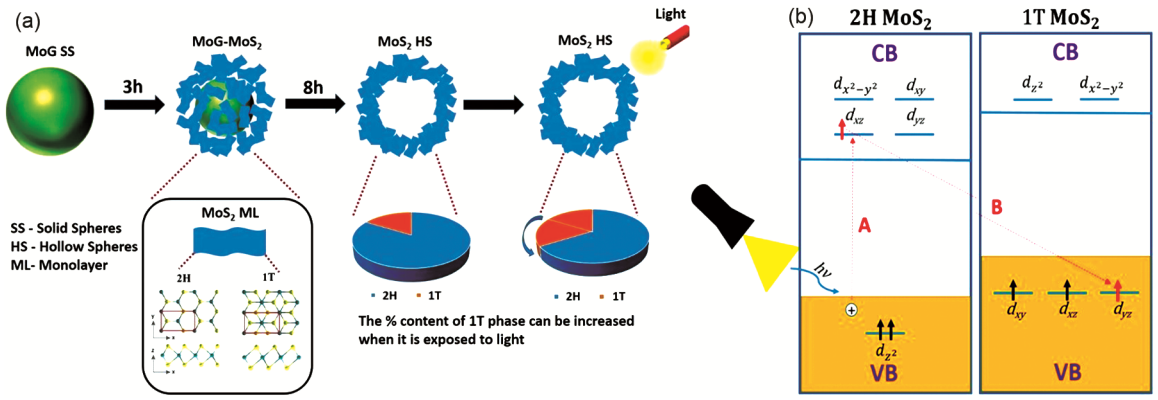

Fig. 5 — Light induced phase transition to improve the phase purity of 1T MoS_2. (a) Mechanistic phase transition of 2H to 1T MoS_2 upon light irradiation

= ½ for allowed direct transition[30]. Fig. 4(b & c) show the Tauc plot of 3h (2H) and 8h (1T + 2H) sulphidated MoS_2 respectively. The extrapolation of the linear portion of the Tauc plot will intercept the hν-axis to give the values of E_g. From the plot, the E_g values of 3h (2H) and 8h (1T + 2H) sulphidated MoS_2 are obtained as 2.7 eV and 1.68 eV respectively. The reduction of E_g value during the phase transition suggests a decrease in semiconducting behavior and an enhancement of metallic character. Although this reduction is not sufficient to reach the ideal E_g value of 0 for a metal, it suggest a conversion from the 2H to the 1T phase and the existence of 1T + 2H phase mixture for the ball-in-ball 8h sulphidated MoS_2. Similar observations of 2H and 1T phase mixtures and reduced E_g values in the 1T metallic phase have been reported[33-36].

The phase purity of the 1T phase could further be enhanced by light induced phase transition as shown in Fig. 5. Fig. 5(a) shows the hierarchical way of carrying out phase transition through sulphidation and further escalate by light irradiation to increase the percentage content of 1T phase MoS_2. Fig. 5(b) shows the mechanistic phase transition of 2H to 1T MoS_2 under light irradiation. 2H MoS_2 exhibits D_{3h} crystal symmetry and the five 4d Mo orbitals are split into three groups: lowest energy a orbital ($4d_z^2$) in the valence band (VB) and 2 fold degenerate e' orbitals ($4d_{xz}$ and $4d_{yz}$) and e'' orbitals ($4d_{x^2-y^2}$ and $4d_{xy}$) occupied the higher energy conduction band (CB). Both the two 4d electrons of Mo^{4+} ion occupy the lowest energy $4d_z^2$ orbital and the higher energy e' and e'' orbitals are left completely empty. The fully filled $4d_z^2$ orbital in the VB is responsible for the semiconducting nature of 2H MoS_2. However, 1T MoS_2 has a centrosymmetric O_h symmetry and the crystal field splits the Mo 4d orbitals into two groups: the lower energy t_{2g} orbitals ($4d_{xy}$, $4d_{yz}$ and $4d_{xz}$) and the higher energy e^*_g orbitals ($4d_z^2$ and $4d_{x^2-y^2}$). In this case, the two Mo 4d-electrons half-filled the 2 out of the 3 degenerate t_{2g} orbitals. Hence, one t_{2g} orbital is completely vacant which indicates that the VB is partially filled exhibiting the metallic behavior of 1T MoS_2[37-38]. In comparison, the $4d_z^2$ orbital of 2H MoS_2 has slightly lower energy than the t_{2g} orbitals of 1T MoS_2. Eventually, the total energy of Mo 4d electrons is also lesser in 2H MoS_2 exhibiting the 2H phase thermodynamically favored compared to the 1T phase. Upon light irradiation, an electron in the VB of 2H MoS_2 gets excited into the high energy e' orbitals which is much higher than $4d_z^2$, destabilizing the 2H phase, as shown by Fig. 5(b). On the other hand, in 1T MoS_2, all the degenerate t_{2g} orbitals are occupied by electrons and attain the stable half-filled electronic configuration. The t_{2g} orbitals in 1T MoS_2 have much lower energy than the e' orbitals of 2H MoS_2. Hence, the overall total energy of the d^3 configuration is relatively lower in the 1T phase and the probability of electron transfer from the e' orbitals of the 2H phase to the t_{2g} orbitals of the 1T phase would be more and shown by Fig. 5(b). This forms the basis of the light-induced phase transition from 2H to 1T MoS_2[39-40].

4 Conclusion

In summary, flower decorated and ball-in-ball MoS_2 heterostructures were synthesized by a facile solvothermal method followed by subsequent sulphidation for 3h and 8h respectively. Nanoflower heterstructure exhibits semiconducting 2H phase whereas ball-in-ball heterostructure exhibits metallic 1T phase. XRD, Raman, FESEM and UV measurements analyses confirmed the mixing of

semiconducting (2H) and metallic (1T) phases in 8h sulphidated ball-in-ball MoS_2. E_g value of 3h sulphidated MoS_2 (2H) lies in the semiconductor region and upon phase transition, the E_g value reduces for 8h sulphidated MoS_2 (2H-1T). It is expected that the 1T phase purity could further be enhanced by light-induced phase transition. Both the phases has their own unique characteristics that may be used in different applications. In addition, the highly conductive 1T MoS_2 could be employed in clean energy harvesting for future energy storage and environment remediation.

References

1 Wilson J A & Yoffe A D, *Adv Phys*, 18 (1969) 193.
2 Niebur A, Soll A, Haizmann P, Strolka O, Rudolph D, Tran K, Renz F, Frauedorf A P, Hubner J, Peisert H, Scheele M & Lauth J, *Nanoscale*, 15 (2023) 5679.
3 Boulet I, Pascal S, Bedu F, Ozerov I, Ranguis A, Leoni T, Becker C, Masson L, Matkovic A, Teichert C, Siri O, Attaccalite C, Huntzinger J R, Paillet M, Zahab A & Parret R, *Nanoscale Adv*, 5 (2023) 1681.
4 Splendian A, Sun L, Zhang Y, Li T, Kim J, Chim C Y, Galli G & Wang F, *Nano Lett*, 10 (2010) 1271.
5 Dutta R, Bala A, Sen A, Spinazze M R, Park H, Choi W, Yoon Y & Kim S, *Adv Mater*, 35 (2023) 2303272.
6 Yu J, Wu S, Zhao X, Li Z, Yang X, Shen Q, Lu M, Xie X, Zhan D & Yan J, *Nanomaterials*, 13 (2023) 2843.
7 Wei Z, Li B, Xia C, Cui Y, He J, Xia J B & Li J, *Small Meth*, 2 (2018) 1800094.
8 Geng X M, Zhang Y L, Han Y, Li J X, Yang L, Benamara M, Chen L & Zhu H L, *Nano Lett*, 17 (2017) 1825.
9 Mak K F, Lee C, Hone J, Shan J & Heinz T F, *Phys Rev Lett*, 105 (2010) 136805.
10 Lee K, Kim H Y, Lotya M, Coleman J N, Kim G T & Duesberg G S, *Adv Mater*, 23 (2011) 4178.
11 Yu X Y, Hu H, Wang Y W, Chen H Y & Lou X W, *Angewandte Chem*, 54 (2015) 7395.
12 Geng X, Sun W, Wu W, Chen B, Al-Hilo A, Benamara M, Zhu H, Watanabe F, Cui J & Chen T P, *Nature Commun*, 7 (2016) 10672.
13 Chang K, Hai X, Pang H, Zhang H, Shi L, Liu G, Liu H, Zhao G, Li M & Ye J, *Adv Mater*, 28 (2016) 10033.
14 Yin Y, Han J, Zhang Y, Zhang X, Xu P, Yuan Q, Samad L, Wang X & Zhang Z, *J Am Chem Soc*, 138 (2016) 7965.
15 Saliba M, Atanas J P, Howayek T M & Habchi R, *Nanoscale Adv*, 5 (2023) 6787.
16 Gan X, Zhao H, Lo T W, Ho K H W, Lee L Y S, Lei D & Wong K Y, *ACS Appl Energy Mater*, 1 (2018) 4754.
17 Huang Q, Li X, Sun M, Zhang L, Song C, Zhu L, Chen P, Xu Z, Wang W & Bai X, *Adv Mater Interfaces*, (2017) 1700171.
18 Zhu J, Wang Z, Yu H, Li N, Zhang J, Meng J, Liao M, Zhao J, Lu X, Du L, Yang R, Shi D, Jiang Y & Zhang G, *J Am Chem Soc*, 139 (2017) 10216.
19 Yin X, Tang C S, Wu D, Kong W, Li C, Wang Q, Cao L, Yang M, Chang Y H, Qi D, Ouyang F, Pennycook S J, Feng Y P, Breese M B H, Wang S J, Zhang W, Rusydi A & Wee A T S, *Adv Sci*, 6 (2019) 1802093.
20 Gao B, Du X, Li Y, Ding S, Xiao C & Song Z, *ACS Appl Mater Interfaces*, 12 (2020) 877.
21 Tsikritzis D, Tsud N, Skala T & Sygellou L, *Appl Surf Sci*, 599 (2022) 153896.
22 Wang Z, Liu Y, Li F & Zhao J, *Phys Chem Chem Phys*, 23 (2021) 20107.
23 Yu J, Qian Y, Wang Q, Su C, Lee H, Shang L & Zhang T, *EES Catal*, 1 (2023) 571.
24 Qian Y, Lyu Z, Zhang Q, Lee T H, Kang T K, Sohn M, Shen L, Kim D H & Kang D J, *Micromachines*, 14 (2023) 297.
25 Chang K & Chen W X, *ACS Nano*, 5 (2011) 4720.
26 Zhang S, Zeng Y, Wang Z, Zhang J & Dong G, *Chem Eng J*, 334 (2018) 487.
27 Oo M K, Alallam B, Doolaanea A A, Khatib A, Mohamed F & Chatterjee B, *ACS Omega*, 7 (2022) 27126.
28 Favier I, Pla D & Gomez M, *Catal Today*, 310 (2018) 98.
29 Smigelskas A D & Kirkendall E O, *Trans AIME*, 171 (1947) 130.
30 Mani A D, Li J, Wang Z, Zhou J, Xiang H, Zhao J, Deng L, Yang H & Yao L, *J Adv Ceram*, 11(7) (2022) 1069.
31 Guo B, Li H, Song H, Zhang Y, Lei X, Fu H, Tan Y & Zhu Z, *ACS Appl Mater Interfaces*, 8 (2016) 5517.
32 Li Q, Lu W, Li Z, Ning J, Zhong Y & Hu Y, *Chem Eng J*, 380 (2020) 122544.
33 Zhang P, Yang S, Gomez R P, Ibarluces B, Ma J, Martin R L, Akbar T F, Baraban L, Cuniberti G & Feng X, *Small*, 15 (2019) 190165.
34 Tang Q & Jiang D, *Chem Mater*, 27 (2015) 3743.
35 Khanlary M R, Parhizkari M & Heydari N, *Phys B Cond Matter*, 680 (2024) 415387.
36 Turnbull R, Platas J G, Rodriguez F, Liang A, Popescu C, He Z, Perez D S, Hernandez P R, Munoz A & Errandonea D, *Inorg Chem*, 61 (2022) 3697.
37 Enyashin A N & Seifert G, *Comput Theor Chem*, 999 (2012) 13.
38 Cheng Y, Nie A, Zhang Q, Gan L Y, Shahbazian-Yassar R & Schwingenschlogl U, *ACS Nano*, 8 (2014) 11447.
39 Kan M, Wang J Y, Li X W, Zhang S H, Li Y W & Kawazoe Y, *J Phys Chem C*, 118 (2014) 1515.
40 Byrley P, Liu M & Yan R, *Front Chem*, 7 (2019) 442.